Computation of Dynamic Stall of a NACA-0012 Airfoil

Yoshifumi Shida*
University of Tokyo, Tokyo, Japan
Kunio Kuwahara†
Institute of Space and Astronautical Science, Tokyo, Japan
Kiyoaki Ono‡
Nihon University, Tokyo, Japan
and
Hideo Takami§
University of Tokyo, Tokyo, Japan

The flowfield around a NACA-0012 airfoil oscillating in pitch about a 0.25 chord is analyzed by solving the two-dimensional compressible Navier-Stokes equations. A block pentadiagonal matrix scheme based on the approximate factorization method is adopted. Two meshes, 161×40 and 321×80, are used. In the case of the coarse mesh, lift stall is captured. In the case of the fine mesh, not only lift stall but also the restoration process of the lift coefficient on the downstroke is captured.

Introduction

An airfoil oscillating in pitch and having a maximum angle of attack greater than the static stall angle experiences peculiar hysteresis in drag, lift, and moment coefficients. It is believed that these phenomena are caused by the formation of leading-edge separation vortices, their convection along the wing surface, and their shedding into the wake.[1]

The linearized unsteady airfoil theory (developed by Theodorsen[2] and von Kármán and Sears[3] and much improved since then by the inclusion of the effects of airfoil thickness, wake deformation, etc.) has been widely used for the analysis of small-amplitude oscillation below the dynamic stall angle. However, in order to treat dynamic stall, an unsteady separated flow theory is needed.

The flowfield around a NACA-0012 airfoil oscillating in pitch was analyzed by Metha[4] by solving numerically the two-dimensional incompressible Navier-Stokes equations. The ψ-ω formulation was used and the flowfield at Reynolds numbers of 5000 and 10,000 was evaluated. In that work, the process of dynamic stall was clearly identified. However, because these computations were very costly in computer time, only the case of high reduced frequency was analyzed. Moreover, Metha's method did not account for compressibility and the maximum Reynolds number in the study was not very high.

In 1981, Ono et al.[5] applied the discrete vortex approximation method to flow about a NACA-0012 airfoil oscillating in pitch. Fairly good results were obtained. For the first time, lift stall was detected by the analysis. Tassa and Sankar[6] used the compressible Navier-Stokes equations to solve for a high Reynolds number flow around an oscillating NACA-0012 airfoil. However, the mesh size used in the simulations was too coarse to analyze the physics of dynamic stall.

McCroskey and Pucci[7] have done intensive experimental research on the dynamic stall process. The deep dynamic stall process associated with a NACA-0012 airfoil oscillating in pitch at low reduced frequency and high Reynolds number was especially well investigated. This process was analyzed by Ono[8] by solving the Navier-Stokes equations numerically. In this calculation, compressibility was taken into account by using a Beam-Warming-Steger code. The process of stall was well simulated, but excessive dissipation yielded results that did not capture the dynamic lift coefficient curve.

In the present study, the same case is analyzed. The Navier-Stokes equations are numerically solved by using the block pentadiagonal matrix inversion scheme[9] based on the approximate factorization method. This scheme is second order in time and the numerical dissipation is carefully controlled. These features of the present scheme are essential for computating strongly unsteady flows having high Reynolds numbers. No turbulence model is used.

Basic Equations

The governing equations are the two-dimensional compressible Navier-Stokes equations in a conservation law form expressed in ξ-η body-fitted coordinate system, that is,

$$\partial_\tau \boldsymbol{q} + \partial_\xi \boldsymbol{M} + \partial_\eta \boldsymbol{N} = 0 \tag{1}$$

where

$$\boldsymbol{M} = E - 1/Re\boldsymbol{R}, \qquad \boldsymbol{N} = F - 1/Re\boldsymbol{S} \tag{2}$$

and τ is the time variable and ξ and η the streamwise and the normal directions, respectively. The flux vectors $\boldsymbol{q}$, E, and F are represented as

$$\boldsymbol{q} = \frac{1}{J}\begin{pmatrix} \rho \\ \rho u \\ \rho v \\ e \end{pmatrix}, \qquad E = \frac{1}{J}\begin{pmatrix} \rho u \\ \rho uU + \xi_x p \\ \rho vU + \xi_y p \\ (e+p)U - \xi_t p \end{pmatrix}$$

$$F = \frac{1}{J}\begin{pmatrix} \rho v \\ \rho uV + \eta_x p \\ \rho vV + \eta_y p \\ (e+p)V - \eta_t p \end{pmatrix} \tag{3}$$

The contravariant velocity components U and V are defined as

$$U = \xi_t + \xi_x u + \xi_y v \qquad V = \eta_t + \eta_x u + \eta_y v \tag{4}$$

Received Dec. 2, 1985; presented as Paper 86-0116 at the AIAA 24th Aerospace Sciences Meeting, Reno, NV, Jan. 6-9, 1986; revision received March 24, 1986.

*Research Associate, Department of Applied Physics.
†Assistant Professor.
‡Research Associate, College of Science and Technology.
§Professor, Department of Applied Physics.

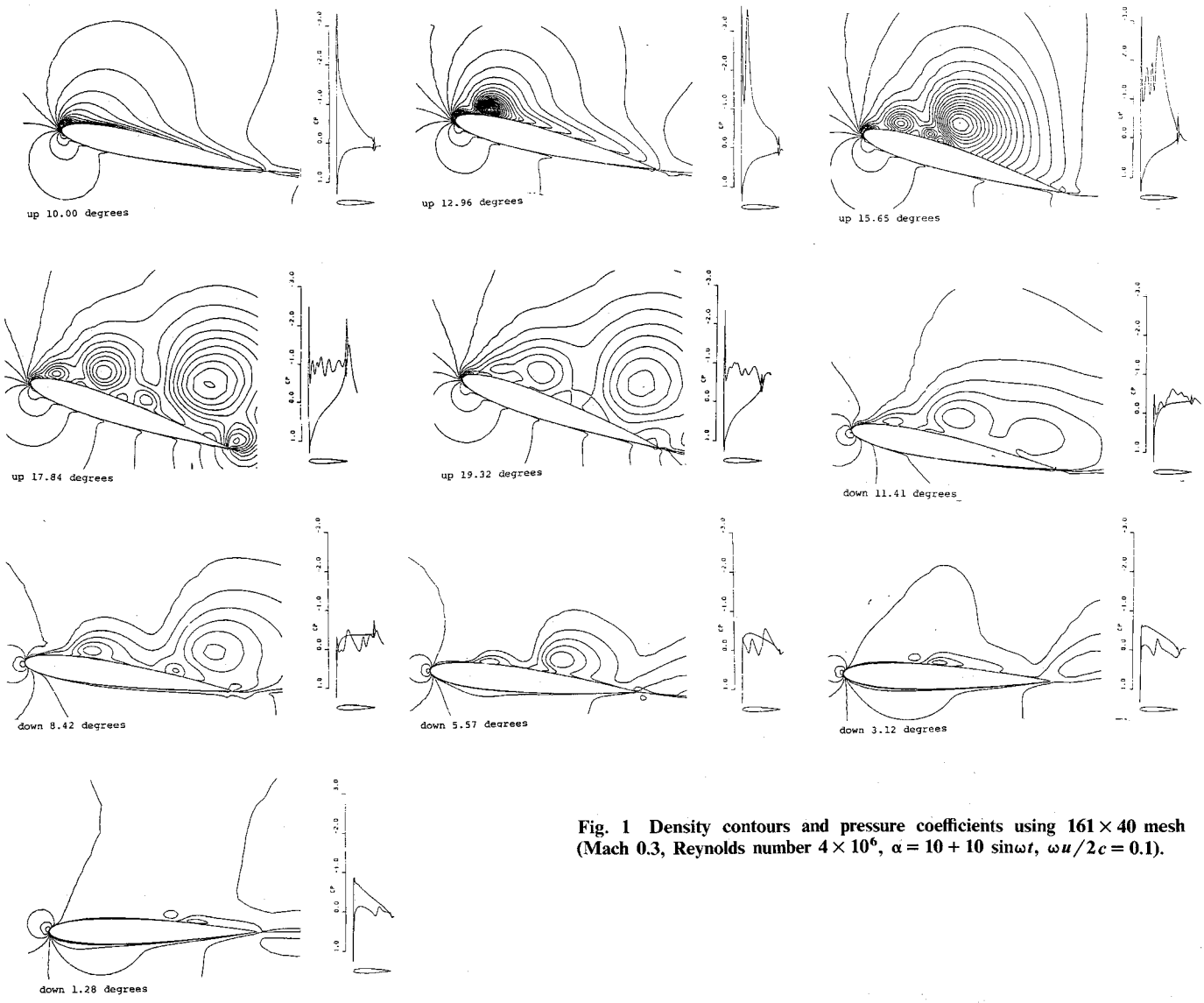

Fig. 1 Density contours and pressure coefficients using 161×40 mesh (Mach 0.3, Reynolds number 4×10^6, $\alpha = 10 + 10 \sin\omega t$, $\omega u/2c = 0.1$).

The metric terms ξ_t, ξ_x, etc., and the transformation Jacobian $J = \xi_x \eta_y - \xi_y \eta_x$ are numerically determined at each time step. The viscous terms are

$$\boldsymbol{R} = \frac{1}{J}\left(\xi_x R + \xi_y S\right) \qquad \boldsymbol{S} = \frac{1}{J}\left(\eta_x R + \eta_y S\right) \tag{5}$$

where

$$R = \begin{pmatrix} 0 \\ \tau_{xx} \\ \tau_{xy} \\ R_4 \end{pmatrix} \qquad S = \begin{pmatrix} 0 \\ \tau_{xy} \\ \tau_{yy} \\ S_4 \end{pmatrix} \tag{6}$$

with

$$\begin{aligned} \tau_{xx} &= (\lambda + 2\mu) u_x + \lambda v_y \\ \tau_{xy} &= \mu(u_y + v_x) \\ \tau_{yy} &= (\lambda + 2\mu) v_y + \lambda u_x \\ R_4 &= u\tau_{xx} + v\tau_{xy} + \alpha \partial_x a^2 \\ S_4 &= u\tau_{xy} + v\tau_{yy} + \alpha \partial_y a^2 \end{aligned} \tag{7}$$

Here

$$\begin{aligned} a^2 &= \gamma(\gamma - 1)\left[e/\rho + \tfrac{1}{2}(u^2 + v^2)\right] \\ \alpha &= kPr^{-1}(\gamma - 1)^{-1} \end{aligned} \tag{8}$$

with k and Pr denoting the thermal conductivity and Prandle number, respectively, and γ the specific heat ratio. Stokes hypothesis $\lambda + \frac{2}{3}\mu = 0$ is assumed. The molecular viscosity μ is determined by using the Sutherland law. No turbulence model is used.

Finite-Difference Algorithm

Many methods have been developed to solve the Navier-Stokes equations. As dynamic stall is a highly unsteady phenomenon, we need to employ a time-accurate scheme. The MacCormack explicit scheme is time accurate, but it is very costly in computer time. The Beam-Warming-Steger method adds second-order differential terms to the implicit side of the algorithm as an artificial dissipation. It thus introduces a diffusive effect similar to molecular diffusion in the case of unsteady computation, which is undesirable for flows with high Reynolds numbers. The diagonal form using a scalar pentadiagonal solver[10] is as accurate as the block pentadiagonal scheme in the sense that both numerical schemes are free of second-order dissipation. However, the time accuracy is reduced from second to first order by diagonalization. Therefore, the block pentadiagonal scheme is employed. This scheme has been successfully applied to the steady-stall problem.[9] The scheme is second-order accurate in time and has no second-order artificial dissipation.

The governing equations are approximated by the following finite-difference method. A three-point backward scheme is

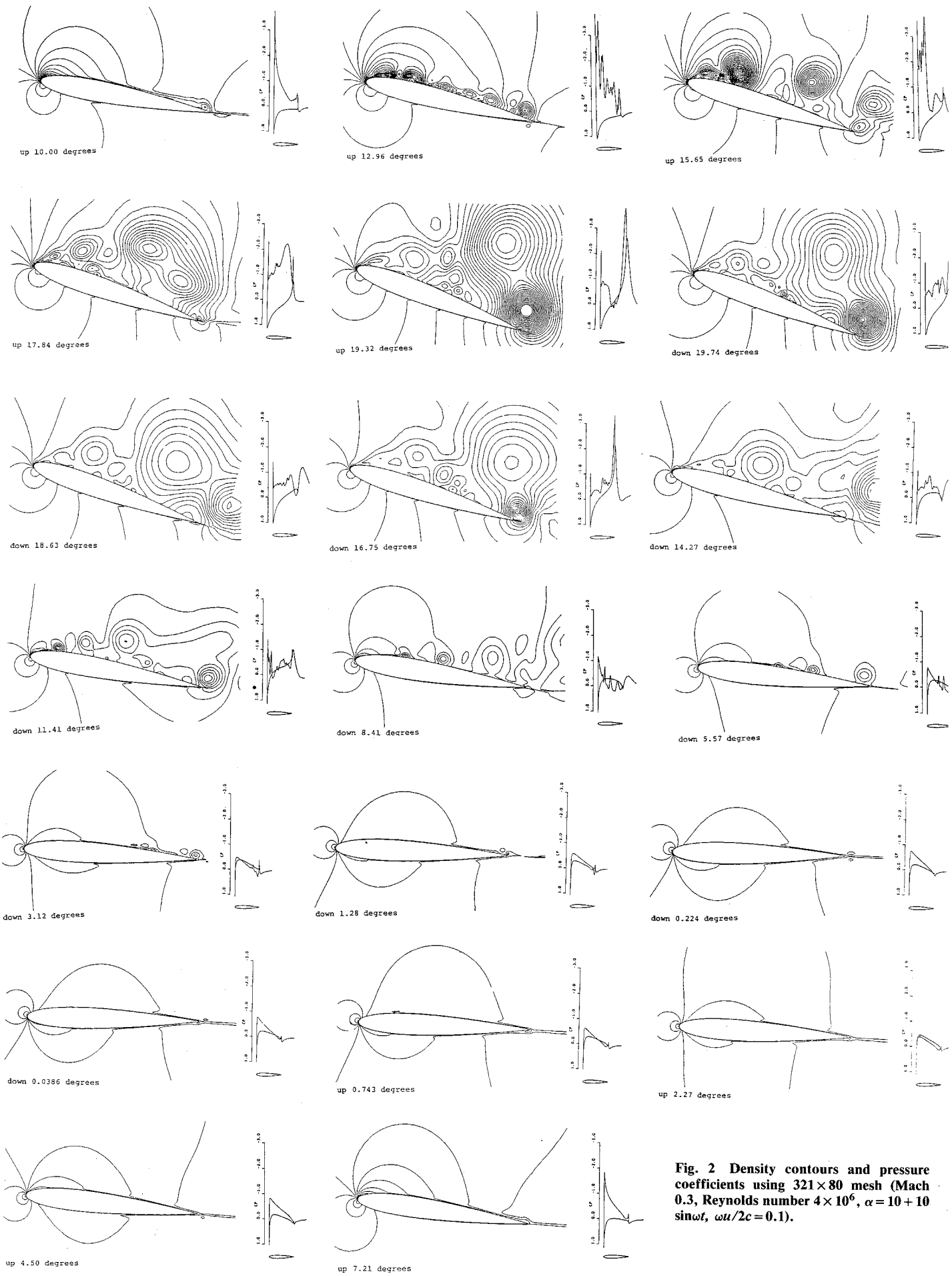

Fig. 2 Density contours and pressure coefficients using 321×80 mesh (Mach 0.3, Reynolds number 4×10^6, $\alpha = 10 + 10 \sin\omega t$, $\omega u/2c = 0.1$).

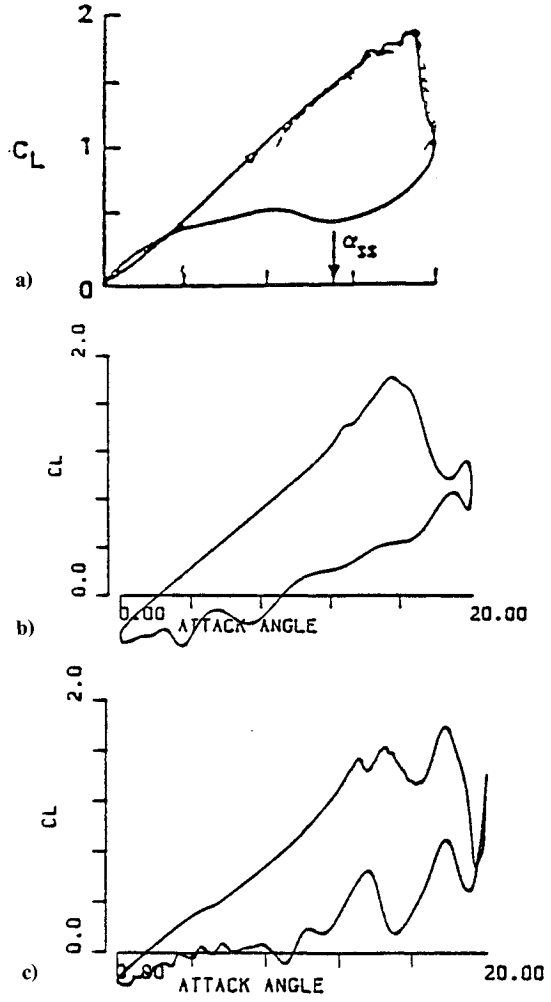

Fig. 3 Life coefficient hysteresis curve vs angle of attack: a) experimental results; b) computational results using 161×40 mesh; c) computational results using 321×80 mesh.

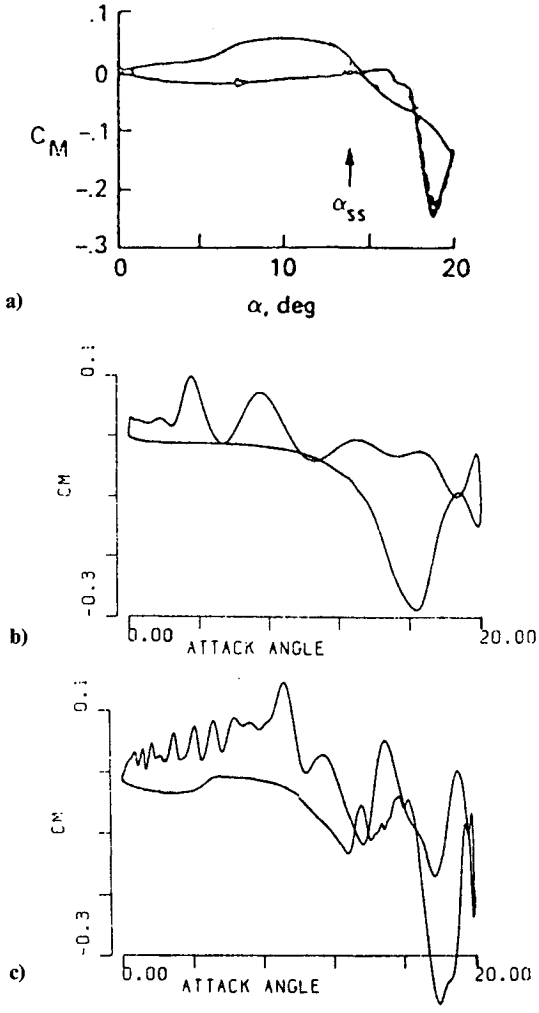

Fig. 4 Moment coefficient hysteresis vs angle of attack: a) experimental results; b) computational results using 161×40 mesh; c) computational results using 321×80 mesh.

applied to Eq. (1), that is,

$$\frac{1}{2}(3q^{n+1} - 4q^n + q^{n-1}) = \frac{3}{2}(q^{n+1} - q^n) + \frac{1}{2}(q^n - q^{n-1})$$
$$= \frac{3}{2}\Delta q^n - \frac{1}{2}\Delta q^{n-1}$$
$$= \Delta\tau\left(\frac{\partial q}{\partial t}\right)^{n+1} + \mathcal{O}(\Delta\tau^3)$$
$$= -\Delta\tau\left(\frac{\partial \boldsymbol{M}^{n+1}}{\partial\xi} + \frac{\partial \boldsymbol{N}^{n+1}}{\partial\eta}\right)$$
$$+ \mathcal{O}(\delta\tau^3) \tag{9}$$

The convection terms E and F in $\boldsymbol{M}$ and $\boldsymbol{N}$ are linearized by using the local Taylor expansion about q, that is,

$$E^{n+1} = E^n + \left(\frac{\partial E}{\partial q}\right)^n \Delta q^n + \mathcal{O}(\Delta\tau^2)$$

$$F^{n+1} = F^n + \left(\frac{\partial F}{\partial q}\right)^n \Delta q^n + \mathcal{O}(\Delta\tau^2) \tag{10}$$

The viscous terms R and S can be divided into two parts, that is, R_ξ and S_ξ consisting of only ξ-derivative terms and R_η and S_η involving only η derivatives. The same linearization is applied to R_ξ and S_η as

$$R_\xi^{n+1} = R_\xi^n + \left(\frac{\partial R_\xi}{\partial q}\right)^n \Delta q^n + \mathcal{O}(\Delta\tau^2)$$

$$S_\eta^{n+1} = S_\eta^n + \left(\frac{\partial S_\eta}{\partial q}\right)^n \Delta q^n + \mathcal{O}(\Delta\tau^2) \tag{11}$$

The other viscous terms S_ξ and R_η are lagged in time, giving explicit expressions

$$R_\eta^{n+1} = R_\eta^n + \mathcal{O}(\Delta\tau) \qquad S_\xi^{n+1} = S_\xi^n + \mathcal{O}(\Delta\tau) \tag{12}$$

Using these approximations, Eq. (9) can be expressed as

$$\left[I + \frac{2}{3}\Delta\tau\frac{\partial}{\partial\xi}\frac{\partial}{\partial q}\left(E - \frac{1}{Re}R_\xi\right)^n\right]$$
$$\times\left[I + \frac{2}{3}\Delta\tau\frac{\partial}{\partial\eta}\frac{\partial}{\partial q}\left(F - \frac{1}{Re}S_\eta\right)^n\right]\Delta q^n$$
$$= -\frac{2}{3}\Delta\tau\left(\frac{\partial}{\partial\xi}\boldsymbol{M} + \frac{\partial}{\partial\eta}\boldsymbol{N}\right)^n + \frac{1}{3}\Delta q^{n-1} + \mathcal{O}(\Delta\tau^2) \tag{13}$$

The accuracy of this scheme is formally first order, but this is only because of Eq. (12), which is the cross-derivative term in the expression for the viscous diffusion that has a minimal effect on the flow. Therefore, this scheme is essentially second

Fig. 5 Density contours at the beginning of separation at stall stage in the case of 321 × 80 mesh.

order. In these expressions, the convective terms are differenced by fourth-order central differencing, that is,

$$\frac{\partial}{\partial \xi} E = \frac{-E_{i+2,j} + 8(E_{i+1,j} - E_{i-1,j}) + E_{i-1,j}}{12(\Delta \xi)}$$

$$\frac{\partial}{\partial \eta} F = \frac{-F_{i,j+2} + 8(F_{i,j+1} - F_{i,j-1}) + F_{i,j-2}}{12(\Delta \eta)} \quad (14)$$

The viscous terms are differenced by second-order, three-point central differencing. Fourth-order artificial dissipations are added to both the implicit and explicit terms. Equation (13) is solved by block pentadiagonal matrix inversion.

Boundary Conditions

On the airfoil surface, the nonslip condition is required for viscous flow. The density is determined from the points next to the body surface. The pressure is computed by solving the normal momentum equation. Uniform flow conditions are imposed at the outer boundaries, except downstream, on which the quantities are extrapolated from those at the grid points just inside the boundary. Five-point differencing is reduced to three-point on this boundary.

Grid Generation

A grid-generation procedure similar to the one reported in Ref. 11 was used. Stationary grids are first constructed for the case with the airfoil at its extreme angle-of-attack position for the prescribed airfoil motion. For these stationary grids, Laplace equations are solved to obtain a smoothed distribution of the interior points and a cubic polynomial is used to determine the distribution of the wake points. For the η direction, the minimum spacing is fixed to 0.00001 of the chord length and the spacing is increased exponentially. This is done by replacing the ξ constant lines.

With the movement of the airfoil, a new grid must be generated at each time step of the computation. To reduce the computational effort that would be required by repeatedly generating grids using the Laplace solver, an interpolation scheme is adopted.[11] The instantaneous unsteady grids at intermediate angles of attack are obtained from interpolation between the stationary grids generated with the airfoil at its extreme angles of attack. The interpolation is linear with an instantaneous angle of attack for all grid points. The corresponding transformation matrices and Jacobian are calculated based on the interpolated grid. In this process, the freestream boundary of the grid is held fixed in time and space. The flow far-field boundary conditions are thus easily implemented within the computation.

Results

The flowfield around an oscillating NACA-0012 airfoil is analyzed by solving the Navier-Stokes equations using the outlined scheme. The parameters for the computations are 0.3 Mach number, 4×10^6 Reynolds number, 0.1 reduced frequency (based on half-chord length), an oscillation mode pitching at 0.25 chord, and a 10 ± 10 deg angle of attack. These parameters are the same as in the experiment of McCroskey and Pucci.[7]

Figures 1 and 2 show the density contours and pressure coefficients on the airfoil surface in the dynamic stall process. Figure 1 shows the results using 161×40 mesh points and Fig. 2 the results using 321×80 mesh points. The lift hysteresis curves are presented in Fig. 3. Figure 4 shows the moment hysteresis. Its composition is the same as Fig. 3. These results are obtained by computing two cycles of the dynamic stall process. The results for the second cycle are shown.

In the case of 161×40 mesh points, the leading-edge separation takes place at an angle of attack of about 12 deg on the upstroke. A large vortex is formed and convected along the airfoil surface. It is shed into the wake at an angle of attack of approximately 17 deg. This process corresponds to the lift stall shown in Fig. 3b. This stall is slightly premature compared with the experimental result shown in Fig. 3a. However, the stall process is clearly captured.

In the downstroke, the agreement between the experimental (Fig. 3a) and the computational (Fig. 3b) results is poor. This is because the resolution of the vortices is not fine enough using 161×40 mesh points. In this case, the scale of the computed vortex might be larger than that associated with the real phenomena. Large vortices move slowly. Thus, at low angles of attack on the downstroke cycle, the vortices formed during the stall stage remain on the airfoil surface. They should, however, be convected away. The existence of these vortices makes the life coefficient smaller than the experiment.

In order to improve this point, 321×80 mesh points are used. In the case of 321×80 mesh points, the restoration of the lift coefficient is captured and the agreement with experiment is improved. Using a 161×40 mesh, during the downstroke cycle at 8 deg, fairly large vortices exist on the airfoil surface, which produces a pressure coefficient curve that shows the airfoil is stalled. In contrast, using 321×80 mesh points, only small vortices exist on the airfoil surface, which produce a pressure coefficient curve indicating attached flow. This difference is due to resolution of the fine flow structure. The fine mesh can resolve the small vortices. Small vortices are convected away in shorter time, thus transforming the separated flow into one that is attached.

The fine resolution also influences the stall process during the upstroke cycle. Leading-edge separation occurs at an angle of attack of about 12 deg, the same as the coarse grid computation. A number of small vortices are formed—sc .e of which remain attached to the airfoil surface, while others are shed into the wake at an angle exceeding static stall. This prevents premature lift stall. Deep lift stall takes place at an angle of attack of about 19 deg. Another noteworthy feature is observed at the beginning of separation. The details of the slow process during this portion of the cycle is shown in Fig. 5 in terms of density contours. From this figure, it is observed that separation occurs from both the leading and trailing edges and propagates from the trailing edge to the center of the airfoil.

These computations have been performed on a HITAC S810-20 supercomputer system. The coarse grid results took about 2 h of CPU time per cycle and the case of the fine grids required about 6 h CPU time per cycle. The memory space used was 16 M bytes for the fine-grid case. The time step used was 0.005. It took 20,944 time steps per cycle.

Conclusion

The flowfield around a NACA-0012 airfoil oscillating in pitch of about 0.25 chord is analyzed by numerically solving the two-dimensional compressible Navier-Stokes equations. The block pentadiagonal matrix inversion scheme based on an approximate factorization method is adopted. This scheme is time accurate; thus, it is suitable for analyzing the unsteady flow associated with dynamic stall. In the case of a 161×40 mesh, lift stall is clearly captured. Moreover, in the case of a 321×80 mesh, the restoration of the lift coefficient during the downstroke cycle is clearly captured. In this fine-mesh case, the process during the onset of separation is elucidated by computation for the first time.

References

[1] Carr, L.W., McAlister, K.W., and McCroskey, W.J., "Analysis of the Development of Dynamic Stall Based on Oscillating Airfoil Experiments," NASA TND-8382, 1977.

[2] Theodorsen, T., "General Theory of Aerodynamic Instability and the Mechanism of Flutter," NACA Rept. 496, 1935.

[3] von Kármán, T. and Sears, W.R., "Airfoil Theory for Nonuniform Motion," *Journal of the Aeronautical Sciences*, Vol. 5, no. 10, 1938.

[4] Mehta, U.B., "Dynamic Stall of an Oscillating Airfoil," AGARD Paper 23, 1977.

[5] Ono, K., Kuwahara, K., and Oshima, K., "Numerical Analysis of Dynamic Stall Phenomena of an Oscillating Airfoil by the Discrete Vortex Approximation," *Proceedings of 7th ICNMFD*, Springer-Verlag, New York, 1981.

[6] Tassa, Y. and Sankar, N.L., "Dynamic Stall of NACA0012 Airfoil," AIAA Paper 81-1289, 1981.

[7] McCroskey, W.J. and Pucci, S.L., "Viscous-Inviscid Interaction on Oscillating Airfoils," AIAA Paper 81-0051, 1981.

[8] Ono, K., "Numerical Study on Dynamic Stall Process of a NACA0012 Airfoil," AIAA Paper 85-0128, 1985.

[9] Shida, Y. and Kuwahara, K., "Computational Study of Unsteady Compressible Flow around an Airfoil by a Block Pentadiagonal Matrix Scheme," AIAA Paper 85-1692, 1985.

[10] Pulliam, T.H. and Steger, J.L., "Recent Improvements in Efficiency, Accuracy, and Convergence for Implicit Approximate Factorization Algorithms," AIAA Paper 85-0360, 1985.

[11] Chyu, W.J., Davis, S.S., and Chang, K.S., "Calculation of Unsteady Transonic Flow over an Airfoil," *AIAA Journal*, Vol. 19, June 1981, pp. 684-690.